Journal of Nuclear Materials 385 (2009) 606–614

Contents lists available at ScienceDirect

Journal of Nuclear Materials

journal homepage: www.elsevier.com/locate/jnucmat

Grazing-incidence electron microscopy of surface blisters in single- and polycrystalline tungsten formed by H^+, D^+ and He^+ irradiation

Naruaki Enomoto [a,1], Shunsuke Muto [a,*], Tetsuo Tanabe [b], J.W. Davis [c], A.A. Haasz [c]

[a] Department of Materials, Physics and Energy Engineering, Graduate School of Engineering, Nagoya University, Furo-cho, Chikusa-ku, Nagoya, Aichi 464-8603, Japan
[b] Department of Advanced Energy Engineering Science, Kyushu University, Hakozaki, Fukuoka 812-8581, Japan
[c] University of Toronto Institute of Aerospace Studies, 4925 Dufferin St., Toronto, ON, Canada M3H5T6

ARTICLE INFO

Article history:
Received 23 April 2008
Accepted 16 January 2009

ABSTRACT

Blisters on single- and polycrystalline tungsten surfaces formed by hydrogen and helium ion irradiation were investigated by grazing-incidence electron microscopy (GIEM) with an ultra-high-voltage transmission electron microscope. It was found that the blister skin thickness formed by D^+ irradiation of polycrystalline tungsten (PCW) was considerably larger than the calculated ion range of the implants; however, this skin thickness (or blister depth) is not related to the pre-existing grain boundaries in the PCW. Blister formation was also observed with GIEM for single crystal tungsten (SCW) irradiated with H^+, D^+, and He^+. The critical ion fluence for blister formation in SCW is estimated to be $\sim 10^{23}$ $H^+(D^+)/m^2$ for H(D) and $\sim 10^{21}$ He^+/m^2 for He. The size of the blisters and their skin structure depends on the irradiating conditions. Typical skin thickness was about 50–150 nm. Based on the assumption that gas particles (H_2, D_2, and He) accumulate within the blisters during H^+, D^+, and He^+ irradiation, the GIEM measurements provide a means to derive an estimate of the amount of gas so accumulated, by reproducing the observed blister shapes with finite element method (FEM) calculations. From the GIEM images and FEM calculations we have estimated the number of implanted ions being retained in the blisters, and compared these amounts with published retention measurements. A mechanism for the blister formation is proposed based on the present results.

1. Introduction

Blisters, hollow dome-shape protrusions formed by the accumulation of gas particles (H_2, D_2, and He) near the surface regions of materials exposed to energetic hydrogen and/or helium irradiation, potentially can lead to adverse material behaviour, e.g., [1,2]. Previous studies have shown that semiconductors and ceramics, which are thought to be very brittle under externally applied stresses, exhibited distinctive surface blistering associated with extraordinarily large plastic deformations [3,4]. The grazing-incidence electron microscopy (GIEM) method was successfully used to perform non-destructive structural analyses of blisters on silicon and silicon carbide surfaces [3–7]. Estimates of the gas pressure and the amount of gas molecules accumulated in the internal open spaces of the blisters were obtained from 'finite element method' (FEM) computer simulations and experimentally measured mechanical properties using indentation tests [8,9]. Cross-sectional transmission electron microscopy observations of the blisters and their precursors enabled the identification of the blistering mechanism in some detail, starting from bubble formation associated with the implant, gas accumulation, and the effects of chemical reactivity between the injected atoms and target materials [8,9]. Furthermore, molecular dynamics (MD) simulations of plastic deformations of silicon under uniaxial stress suggested that disordered (amorphous) structure without a long-range order allows the materials to be plastically deformed by collective rearrangements of atomic positions within a few atomic distances in a volume of a few nanometers in diameter [10].

In this study, we will apply the blistering mechanism identified above to tungsten. Tungsten has been selected for use in the divertor of the International Thermonuclear Experimental Reactor, ITER [11,12], and as such, has received considerable attention, especially from the viewpoint of tritium retention. In the divertor, tungsten plasma-facing components will be exposed to D^+, T^+, and He^+ irradiation with energies ranging from <100 eV to >1 keV, high enough to cause displacement damage. Systematic studies of depth distributions of hydrogen (deuterium) implanted with >1 keV energy, using secondary ion mass spectroscopy (SIMS) and ion beam techniques (elastic recoil detection analysis, ERDA; and nuclear reaction analysis, NRA) showed that the implanted atoms (H, D) are trapped, not only by vacancy type defects around the expected damage profile, but also at dislocations and extended defects induced by the implanted atoms, and located as far as a few micrometers from

* Corresponding author. Tel.: +81 52 789 5200; fax: +81 52 789 5137.
E-mail address: s-mutoh@nucl.nagoya-u.ac.jp (S. Muto).
[1] Present address: Fujimatsu Plant, TOYOTA AUTO BODY Co., LTD., 100 Kanayama Ichiriyama-cho, Kariya, Aichi 448-8666, Japan.

0022-3115/$ - see front matter © 2009 Elsevier B.V. All rights reserved.
doi:10.1016/j.jnucmat.2009.01.298

the surface, suggesting that the implanted hydrogen penetrates deep inside the bulk [13–17].

Recent studies have shown that blister formation in tungsten can occur during D^+ irradiation even at energies below the displacement threshold (2050 eV for H^+ [18] and 940 eV for D^+ [13]). Blister shapes and sizes depend on the microstructure of the tungsten crystal target and the irradiation temperature [16,19–22]. These observations suggest that diffusion and accumulation of hydrogen via grain boundaries in powder-sintered polycrystalline tungsten (PCW) would play an important role in determining the blister morphology, though such a mechanism would not apply to single crystal tungsten (SCW). Blistering and dislocation loop formation have also been observed in tungsten irradiated with He^+, even at energies below the displacement threshold [23–26], as was seen for hydrogen. The critical He^+ fluence for blistering, however, is about two orders of magnitude lower than that for hydrogen irradiation; the difference might be attributed to differences in atomic size and chemical reactivity with the target matrix.

To study the blistering mechanism in tungsten, which is very closely related to retention of the implanted atoms, it is necessary to examine the internal structure of the blisters. Since the blisters are formed as a result of gas accumulation at a certain depth, direct observation of the blister skin thickness will give the most unambiguous evidence for the gas retention depth. To date, no direct observations of blister skin thicknesses in tungsten have been actually reported, partly because the hard and brittle nature of tungsten blisters has hampered thin foil preparation for TEM observations. In the present study, we conducted GIEM observation of blisters formed by H^+, D^+, and He^+ irradiation of SCW and PCW specimens following the method discussed above, using 'ultra-high-voltage transmission electron microscopy' (HVEM), by taking advantage of its high penetrating power.

2. Experiment

2.1. Specimens

High purity SCW (99.99%) produced by electron beam melting was used in the present experiments. Test specimens were cut into rectangular parallelepiped blocks (2×1 mm^2 and 1 mm thickness) by a diamond-sintered wire saw. One side of each block was electrochemically polished in a 1 wt% NaOH solution. Prior to irradiation, the SCW specimens were heated to ~400 K when the specimens were mounted in order to cure the epoxy adhesive; no further annealing was done. Then, the polished side of the blocks was irradiated with H^+, D^+, or He^+. Ion beam parameters and irradiation temperatures are summarized in Table 1. The specimen temperature for most of the cases reported here was intended to be around room temperature (RT), however, the effect of beam heating led to slightly higher temperatures: about 400 K for H^+ and D^+ and about 320 for He^+; the lower temperature for He^+ is due to the relatively lower He^+ beam current and short implantation times. For most of the SCW specimens the temperature was monitored during irradiation with a K-type thermocouple (chromel–alumel) and the measured temperatures are recorded in Table 1. (For the other cases the temperature was estimated from irradiations at similar conditions.)

To see the effect of grain boundaries on blister structure, polycrystalline tungsten was also exposed to D^+ irradiation. The PCW specimen (~8×10 mm) was 99.95 wt% pure and was cut from a 25 μm sheet produced by Rembar Corp. This specimen was not heated prior to irradiation. The nominal temperature during irradiation was RT, however due to heating by the D^+ beam (fluence of 1×10^{24} D^+/m^2) it was likely to be about 350–400 K. For GIEM analysis the PCW specimen was cut into slender strips of 1×2 mm.

2.2. Ion irradiation

Irradiation of the tungsten specimens was performed with the mass-analyzed dual ion beam accelerator [27] at the University of Toronto Institute for Aerospace Studies generally followed the procedures outlined in [28]. Ions were incident on the specimens at 21° from normal incidence. For implantations at temperatures >400 K, specimens were mounted on a ceramic heater, and their temperature during irradiation was measured with a chromel–alumel thermocouple. Unheated specimens were mounted in the same specimen holder, although a thermocouple was not always present. In order to mount the small SCW pieces in the specimen holder, the SCW specimens were first attached to small pieces of stainless steel foil (~8×8 mm) by a graphite-based epoxy, which was cured in air at 400 K for 4–5 h. For the cases reported here 4.5 keV H_3^+ and 4.5 keV D_3^+ molecular ions were used which upon impact with the target results in three particles, each with ~1.5 keV energy, i.e., 1.5 keV/H^+ and 1.5 keV/D^+. (Here, we use H^+ and D^+ to represent the molecular ion fragments even though not

Table 1
Summary of tungsten irradiation conditions, and GIEM observations.

Specimen #	1	2	3	4	5	6	7	8
Figure number	Fig 2	Fig 3(a)	Fig. 3(b)	Fig. 4(a,b)	Figs. 4(c,d) and 5(a)	Fig. 5(b)	Fig. 5(c)	Figs. 6 and 7
Implant species	D^+	H^+	H^+	D^+	D^+	D^+	D^+	He^+
SCW/PCW	PCW	SCW	SCW	SCW	SCW	SCW	SCW	SCW
Ion energy (keV)	1.5	1.5	1.5	1.5	1.5	1.5	1.5	5.0
Flux (m^{-2} s^{-1})	2.8×10^{19}	2.8×10^{19}	1.5×10^{20}	1.7×10^{20}	1.4×10^{20}	1.3×10^{20}	1.4×10^{20}	5.1×10^{18}
Fluence (m^{-2})	1.0×10^{24}	1.1×10^{23}	1.0×10^{24}	1.0×10^{23}	1.0×10^{24}	1.0×10^{24}	1.0×10^{24}	5.0×10^{21}
Temperature (K)	350–400[a]	~350[a]	360–400	~400[a]	~400	500	700	~300[a]
Base diameter (nm)	100–3000	100–1000	100–1000	100–1000	300–1500			500–1000
Height (nm)	200–700	~150	~300	~200	200–500			~500
Skin thickness (nm)	50–150	Not observable	Not observable	50–100	50–150			50–150
Structure of skin	Uniform Amorphous	–	–	Uniform amorphous (Fig 4(b))	Mixture of amorphous and poly-crystalline fine particles (Fig. 4(d))			Non-uniform poly-crystalline
Blister density (m^{-2})	$\sim 1 \times 10^{12}$	$\sim 3 \times 10^{12}$	$\sim 1 \times 10^{12}$	$\sim 4 \times 10^{12}$	$\sim 2 \times 10^{12}$			$\sim 1 \times 10^{12}$

[a] The temperature of the PCW and some of the SCW specimens was not measured during irradiations; it was estimated from irradiations at similar conditions.

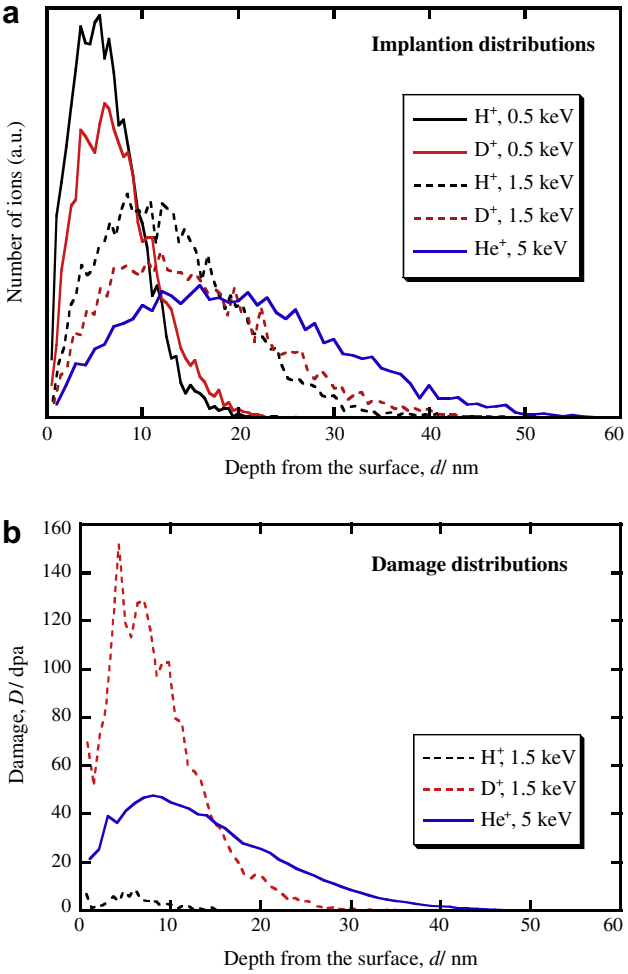

Fig. 1. Depth distributions of: (a) implanted ion concentrations, and (b) ion-induced damage as calculated by SRIM [29] for several incident ion energies. In (b) the vertical axis corresponds to the number of displacements per atom (dpa) for fluences of 1.0×10^{23}/m^2 for H^+ and D^+ and 5.0×10^{21}/m^2 for He^+.

all fragments are charged.) For helium irradiations 5 keV He^+ ions were used.

The ion ranges and damage distributions calculated with a Monte Carlo simulation code, SRIM [29], using a dislocation energy of 40 eV, are shown in Fig. 1(a) and (b), respectively, where the damage distributions are presented in units of displacements per atom (dpa) for fluences of 1.0×10^{23} $H^+(D^+)$/m^2 and 5.0×10^{21} He^+/m^2.

2.3. Grazing-incidence electron microscopy

Grazing-incidence electron microscopy was performed at Nagoya University. The irradiated specimens were mounted on a single-hole grid with the polished and irradiated side exposed to the electron beam at grazing incidence. The specimens were observed with both JEM200CX (operated at 200 kV) and H-1250ST (1 MV) transmission electron microscopy (TEM). The GIEM technique is applicable to non-destructive structural analysis of small (<1 μm) surface protrusions, without any particular specimen preparation technique, usually required for TEM observation [3,4].

3. Results and discussion

3.1. H^+ and D^+ irradiation

3.1.1. Polycrystalline tungsten

GIEM images (with TEM operated at 200 kV) of a PCW (specimen #1) surface irradiated with D^+ at about 350–400 K to a fluence of 1.0×10^{24}/m^2 are shown in Fig. 2(a) and (b); 2(b) is an enlarged image of 2(a). Previous studies of semiconductors and ceramics indicated that the implant atoms/molecules (gas phase) were accumulated around the ion range peak or around the damage peak, and it is this depth that determined the final skin thickness of the blisters [3–8,10]. It is thus expected from Fig. 1 that the skin thickness of the tungsten blisters would be about a few nanometers, which should be transparent to the 200 keV incident electrons [30], and one should be able to observe the microstructure of the skin. However, it was found that the blister skin completely blocked the transmission of the electrons, as clearly shown by the dark contrast (shadow) in the enlarged image in Fig. 2(b). This indicates that the skin thickness is much larger than expected based on the SRIM-calculated ion implantation range, in contrast to what has been observed for Si and SiC [3–8,10].

To improve the ability to see through the blisters, subsequent images were observed with the ultra high-voltage TEM (HVEM) operated at 1 MV. The blister images of the PCW (specimen #1) observed with HVEM are now able to reveal the internal structure of the blisters, as shown in Fig. 2(c) and (d). The thickness of the blister skin ranges between 50 and 150 nm, much thicker than that expected from the calculated ion ranges of the implants. Note that Fig. 2(d) is an enlarged image of Fig. 2(c) and includes an inset of the diffraction pattern from one of the blister skins; the pattern reveals an amorphous structure. The GIEM observations and the

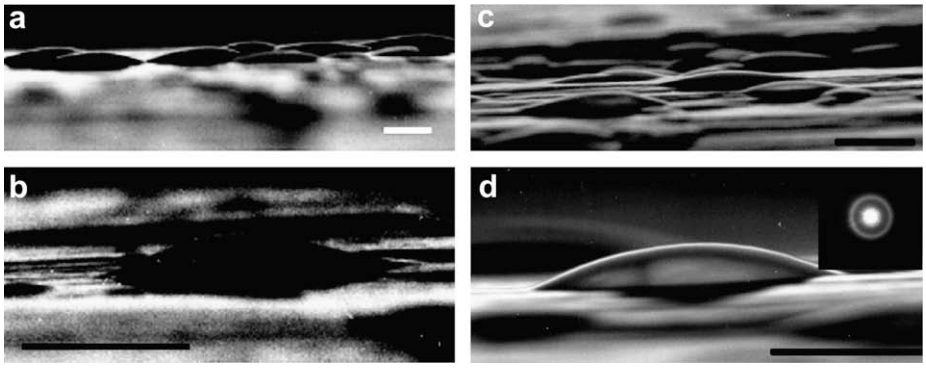

Fig. 2. GIEM images of surface blisters in PCW tungsten (specimen #1) formed by 1.5 keV/D^+ irradiation at about 350–400 K to a fluence of 1.0×10^{24} D^+/m^2, observed at accelerating voltages of 200 kV in (a, b) and 1 MV in (c, d). Images in (b) and (d) are magnified parts of (a) and (c). Note: the specimen number given here and also in subsequent figures correspond to those given in Table 1. The scale bars represent 1 μm.

corresponding ion-beam parameters for all irradiation cases presented in this study are summarized in Table 1.

3.1.2. Single crystal tungsten

GIEM images of surface blisters in SCW are shown in Fig. 3 for H^+-irradiation at about 350–400 K to two fluences (specimens #2 and #3). Similarly, SCW blister images for D^+-irradiation at ~400 K for the same two fluences as the H^+ cases are shown in Fig. 4 (specimens #4 and #5). Comparing the respective H^+/D^+ GIEM images for irradiations at $\sim 1.0 \times 10^{23}$ $H^+(D^+)/m^2$ in Figs. 3(a) and 4(a)) with the H^+/D^+ GIEM images for $\sim 1.0 \times 10^{24}$ $H^+(D^+)/m^2$ in Figs. 3(b) and 4(b)), it is apparent that both the size and density of the blisters are larger for the higher fluence cases. From these images, an approximate critical fluence for the onset of blistering in SCW is estimated to be at or below $\sim 1.0 \times 10^{23}/m^2$ for both H^+ and D^+ irradiations at $\leqslant$400 K – consistent with previously reported values [21,31]. Since the height of the H^+-irradiated blisters (Fig. 3) is too small to be discernable, it is not possible to see the internal structure of the blisters. Considering the small amount of displacement damage introduced by the incident H^+ ions, see Fig. 1, it might be expected that the blister skin structure would remain single crystalline, though containing a high density of defects.

GIEM images of surface blisters produced in specimen #4 by D^+ irradiation at ~400 K and 1.0×10^{23} D^+/m^2 fluence are shown in Fig. 4(a and b). Judging from the electron diffraction pattern inset in Fig. 4(b), the structure of these blisters appears to be 'amorphous' with a smooth uniform thickness. For comparison, blisters produced on specimen #5 by the higher fluence (1.0×10^{24} D^+/m^2 at 400 K) irradiation are shown in Fig. 4(c) and (d). In contrast with the lower fluence case, the structure of these blister skins seems to contain 'fine crystalline particles,' which are evident in the enlarged image in Fig. 4(d), implying that some re-crystallization might have occurred. (These features are very similar to those seen in blisters formed in silicon [3,4].)

It should be noted that the observed skin thicknesses observed for D^+ irradiations of SCW specimens #4 and #5 (Fig. 4(a)–(d)) are similar for both fluence cases and range from 50 to 150 nm; also see Table 1. These thicknesses are nearly one order of magnitude larger than the expected ion range of D^+ and H^+, unlike the case in silicon and silicon carbide, where the blister thickness was similar to the hydrogen and helium ion ranges [3–7]. Moreover, the skin thicknesses observed in the present study are similar for both single- and polycrystalline specimens, e.g., compare PCW specimen #1 (Fig. 2) and SCW specimen #5 (Fig. 4(c) and (d)), both irradiated with 1.5 keV/D^+ at ~400 K to a fluence of 1.0×10^{24} D^+/m^2. This near-surface presence of implanted D is consistent with NRA measured depth distributions of trapped D in PCW (the same material as the one used in the present study) irradiated with 500 eV and 1 keV D^+ at 300 K [17]. While the ion range at these energies is about 10 nm, the trapped D profile extends to 200–300 nm and peaks around 80 nm [17]. We note, however, that in addition to near-surface diffusion of D leading to the blisters observed in the present study, D diffusion further into the bulk at 500 K, possibly along grain boundaries, of PCW also leads to blister formation, with thicknesses on the order of the depthwise grain dimension, e.g., Haasz et al. observed blisters with several micrometer thickness [16].

GIEM images of blisters produced by 1.5 keV/D^+ irradiation of SCW with 1.0×10^{24} D^+/m^2 are shown in Fig. 5 for three different temperatures: specimen #5 at ~400 K in Fig. 5(a), which is the same as Fig. 4(c); specimen #6 at ~500 K in Fig. 5(b); and specimen #7 at 700 K in Fig. 5(c). The growth of blisters – both height and density – appears to be suppressed with increasing irradiation temperature. The blisters at 500 and 700 K do not reveal internal structures even with 1 MeV electrons, implying that the blister skin thickness is likely to be larger at these elevated temperatures than that seen for the ~400 K irradiation in Fig. 4(c).

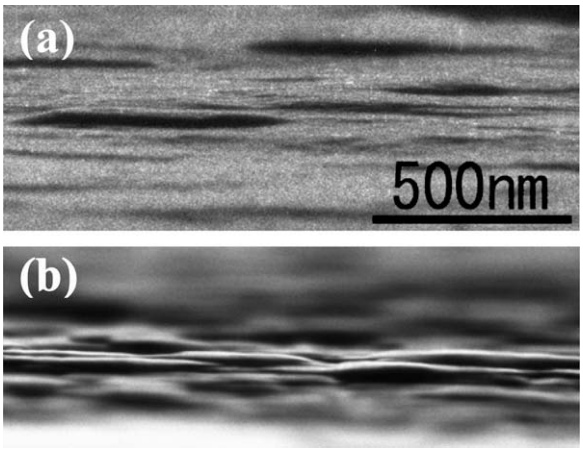

Fig. 3. GIEM images of surface blisters in SCW formed by 1.5 keV/H^+ irradiations: (a) specimen #2 irradiated at ~350 K to a fluence of 1.1×10^{23} H^+/m^2; (b) specimen #3 irradiated at 360–400 K and 1.0×10^{24} H^+/m^2. The scale bar applies to both (a) and (b).

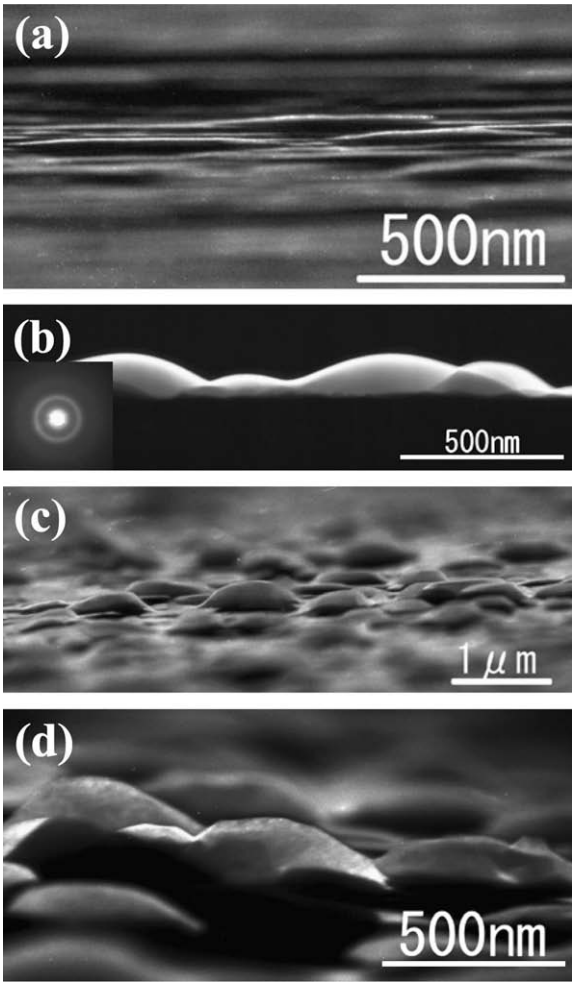

Fig. 4. GIEM images of surface blisters in SCW formed by 1.5 keV/D^+ irradiations: (a,b) specimen #4 irradiated at ~400 K to a fluence of 1.0×10^{23} D^+/m^2, with the inset in (b) showing an 'amorphous' structure in the electron diffraction pattern for a selected area of the blister skin; (c, d) Specimen #5 irradiated at ~400 K and 1.0×10^{24} D^+/m^2.

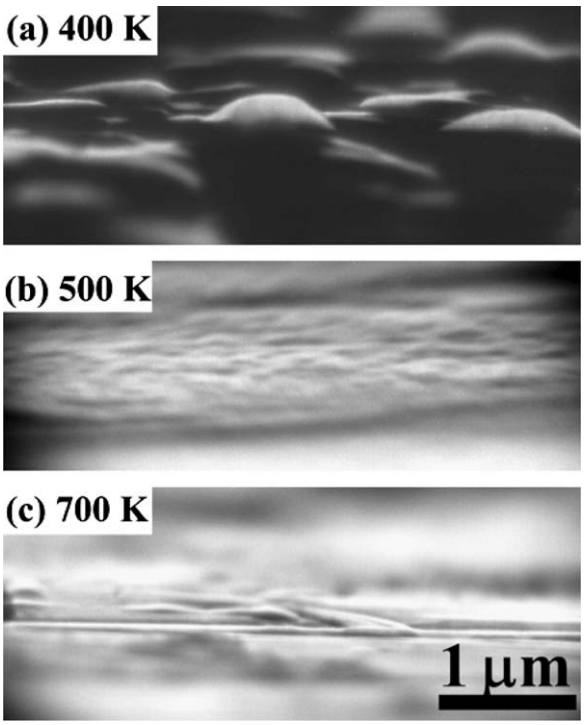

Fig. 5. GIEM images of surface blisters in SCW formed by D^+ irradiation with a fluence of 1.0×10^{24} D^+/m^2 at three irradiation temperatures: (a) specimen #5 at ~400 K; (b) specimen #6 at ~500 K; and (c) specimen #7 at ~700 K.

3.2. He^+ irradiation

GIEM images of blisters formed by 5 keV He^+ irradiation of SCW (specimen #8) at ~300 K and a fluence of 5.0×10^{21} He^+/m^2 are shown in Fig. 6. Since no blisters with appreciable size were observed in a specimen irradiated with similar conditions as specimen #8, but to a lower fluence of 1.0×10^{21} He^+/m^2 (not shown), the critical dose for blistering by He^+ irradiation is considered to be around 1.0×10^{21} He^+/m^2, which is lower by nearly two orders of magnitude than that for H^+ and D^+ irradiations of SCW. Larger blisters are sometimes seen, as shown in Fig. 6(b), with variations in contrast which indicate that the internal blister structure is not of uniform thickness. An enlarged transmission dark-field image of such a large He-blister is shown in Fig. 7(a). It should be noted that the thickness of the skin is again much larger than the calculated ion range peak location in Fig. 1. The transmission electron diffraction pattern inset in Fig. 7(a) clearly shows that the skin structure is polycrystalline. Furthermore, no bubbles were observed in the blister skin, as seen in a high-magnification high-resolution lattice image in Fig. 7(b), unlike previous observations for sintered polycrystalline tungsten [32].

For He^+ irradiations at 700 K (not shown), blistering was suppressed as was also seen for H^+ and D^+ irradiations in Fig. 5. No blisters large enough to observe the substructures of the skins were detected; only undulated surface structures were observed.

4. Possible blister formation mechanism in single crystal tungsten

Here, we attempt to explain why the blister cap thickness is much larger than the SRIM-calculated range of the implanted ions. We base our discussion on experimental observations of D accumulation beyond the implant zone (to ~500 nm) for D^+ irradiation of PCW at 300 K [17]. The discussion could be applied to both SCW and PCW since the blister depth (~50–150 nm) is much smaller

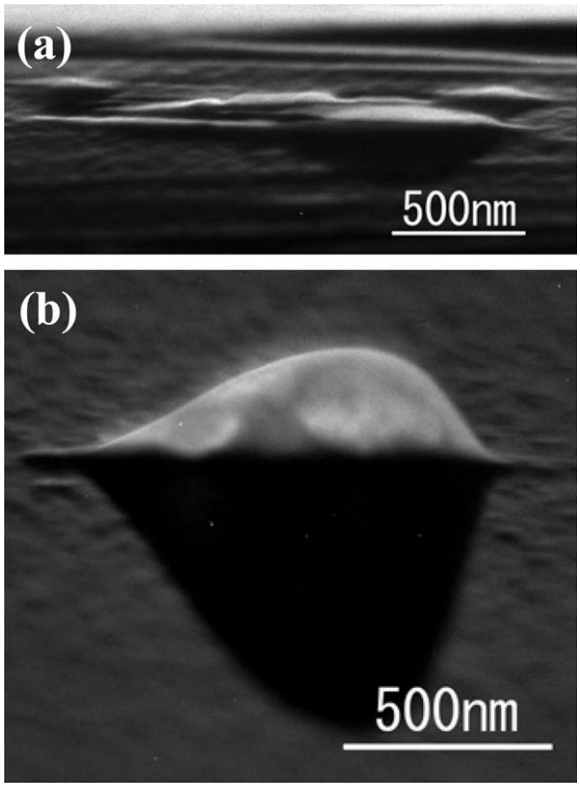

Fig. 6. (a) GIEM images of surface blisters in SCW (specimen #8) formed by He^+ irradiation with a fluence of 5.0×10^{21} He^+/m^2 at ~300 K. (b) Enlarged image of one of the well grown blisters with a discernable skin structure on top of the blister.

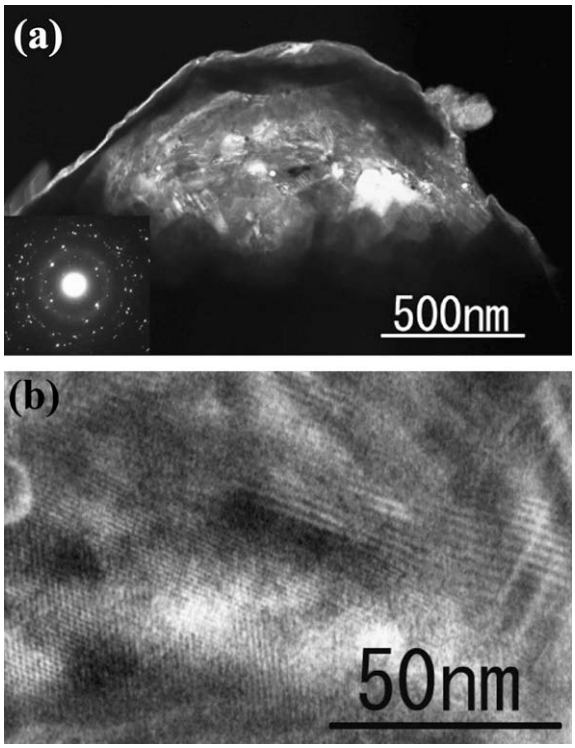

Fig. 7. (a) Transmission dark-field image of He-blister on specimen #8. The corresponding electron diffraction pattern (inset) shows a polycrystalline structure. (b) High resolution lattice image of a portion of the image in (a).

than the grain depth of ~10 μm of the PCW [16] used in this study. However, we recognize that in the case of PCW materials, blister formation due to grain boundary diffusion and D accumulation at grain boundaries might also occur. The first step in our approach is to identify a mechanism that allows the thermalized implanted atoms to diffuse a considerable distance beyond the ion range and accumulate there. A conventional mechanism for hydrogen retention is hydrogen trapping and trap evolution by cavity formation, introduced by irradiation and the super-saturation of hydrogen within the tungsten lattice, e.g., [33–36]. Hydrogen trapping occurs at impurities, dislocations, vacancies, grain boundaries and other crystal defects within the implantation zone, e.g., [37,38]. If all the traps become filled, and the flux of hydrogen is larger than the rate of hydrogen diffusion out of the implantation zone, there will exist a local super-saturation of mobile hydrogen due to its very low solubility [37]. Hydrogen introduced by prolonged irradiation pushes the preexisting distribution of trapped atoms deeper into the specimen, as schematically shown in Fig. 8. Such near-surface trapping beyond the implantation zone, but within a particular grain, was seen by NRA in PCW [17].

The presence of trapped hydrogen in the tungsten lattice leads to swelling of the tungsten, and lateral compressive stresses within the surface layer [16]. The lateral compressive stress model for blister formation has already been well developed [33] for cases where the blister skin thickness is comparable to the ion range. In the current case, however, the implantation depth is <10 nm,

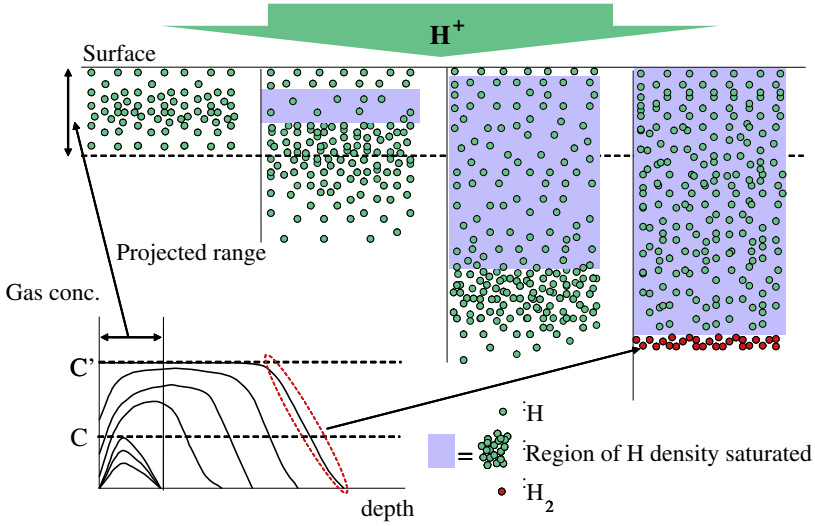

Fig. 8. Schematic diagram showing a potential model of the blistering process by H^+, D^+ or He^+ irradiation of tungsten, with fluence increasing from left to right. The scales correspond to the experimental parameters in this study, 1.5–5.0 keV. See text for detail.

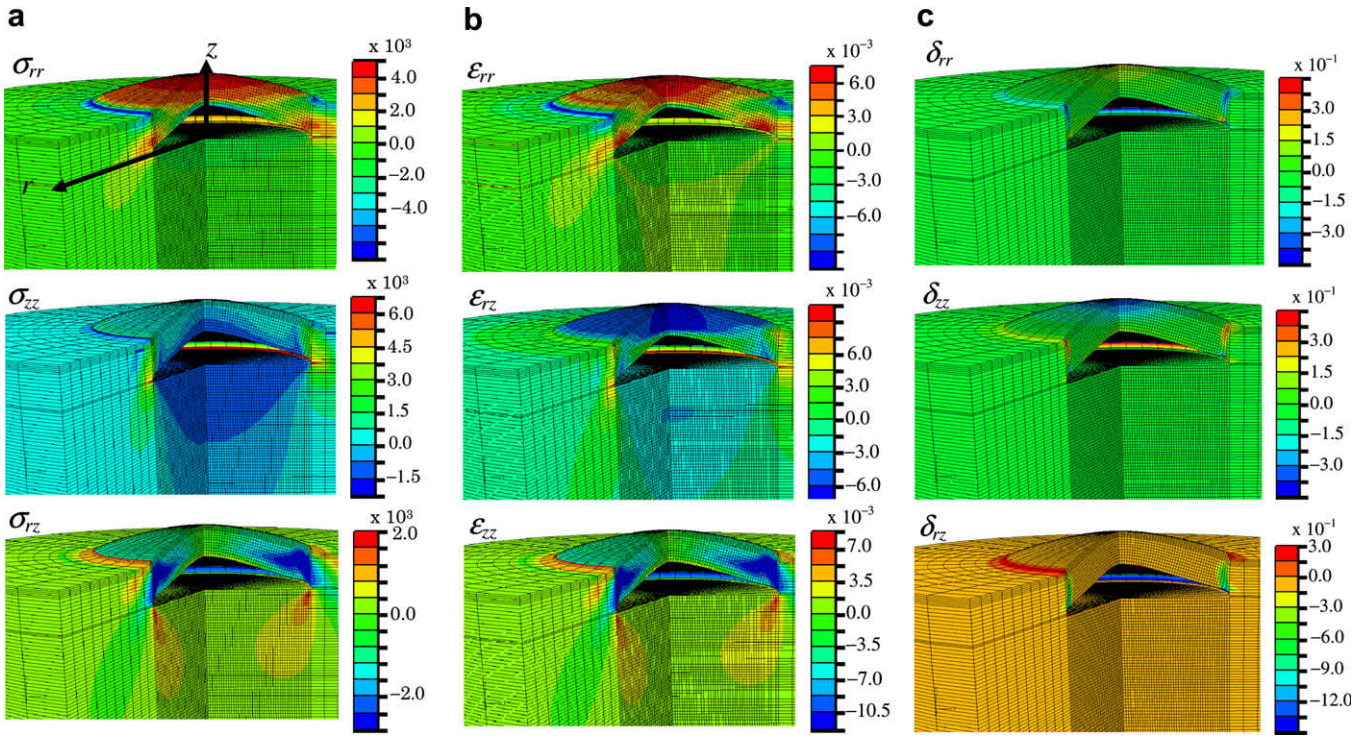

Fig. 9. FEM simulation results of H-blisters, showing distributions of (a) stress (σ_{ij}) in units of Pa; (b) elastic strain (ε_{ij}); and (c) plastic strain (δ_{ij}).

while the blister skin thickness is 50–150 nm. We, therefore, postulate that the tungsten lattice is able to withstand lateral stresses in the thin surface layers comparable to the implantation depth. However, as the hydrogen diffuses further into the bulk, the thickness of the compressive layer increases, until the tungsten can no longer withstand the stress. At this point, local delamination occurs, followed by mobile H atoms entering the cavity and recombining to form H_2, which will fill the resulting cavity and lead to blister formation. We note that in the previously studied cases of Si and SiC the observed blister skin thickness was comparable to the ion implantation depth [3–8,10]. We suggest that, in these cases, the accumulation of H or He within the implantation range leads to sufficient lateral stresses to cause delamination and blister formation.

5. FEM simulation to estimate the gas pressure in the blister

The internal gas pressures of the blisters were estimated by computer simulations based on the finite element method (FEM) in the same manner as was done in the previous study for blisters in silicon [8]. First, a bulk continuum material with a layered structure is set up in the FEM computer code (ABAQUS ver. 6.3 [39]), where each layer has different mechanical properties according to the introduced damage distribution. In the present case the bulk model was divided into four layers, as was done in [8]: the total thickness was set to be 500 nm, and the thickness of each layer was set to be 10, 10, 30, and 450 nm, respectively. The mechanical parameters: Young's modulus, E; and critical yield stress, Y; at each layer were estimated from those measured by the nano-indentation method for an unirradiated specimen and published data of their dependence on irradiation fluence for H^+- and He^+-irradiated tungsten [32,40]. Then, a thin circular opening was introduced at the depth corresponding to the measured skin thickness (for H^+ irradiation, in which the skin thickness could not be experimentally measured, the skin thickness for D^+ irradiation was used), with a diameter that approximates the internal base area of a typical blister observed in the present study. This was followed by allowing the internal hydrostatic pressure to increase until the upper layer was elasto-plastically deformed to the observed blister shape. Since the observed blister skins were amorphous or polycrystalline, the isotropic continuum model with cylindrical symmetry could be applied.

Spatial 3D plots in Fig. 9(a)–(c) show, respectively, the stress, elastic strain, and plastic strain of the simulated blisters, which correspond to a case of H^+ irradiation (SCW specimen #2; energy: 1.5 keV/H^+; fluence: 1.0×10^{23} H^+/m^2; irradiation temperature: ~350 K). Similarly, stress, elastic strain, and plastic strain plots for a case of He^+ irradiation (SCW specimen #8; energy: 5 keV He^+; fluence: 5.0×10^{21} He^+/m^2; temperature: ~300 K) are shown in Fig. 10(a–c). The mechanical and structural parameters of the most damaged regions (5–10 nm from the surface) used for the simulations are given in Table 2. We tried several models with different numbers of layers (2–4), which resulted in similar values within ~10%. The derived parameters (internal pressure in the blister, P; internal blister volume, V; number of molecules contained in the blister, n; and the calculated number of implanted atoms involved in the formation of the blister, N_{calc}) are presented in Table 3, together with the blister number density, ρ, measured from GIEM images. The final internal hydrostatic pressures derived from the

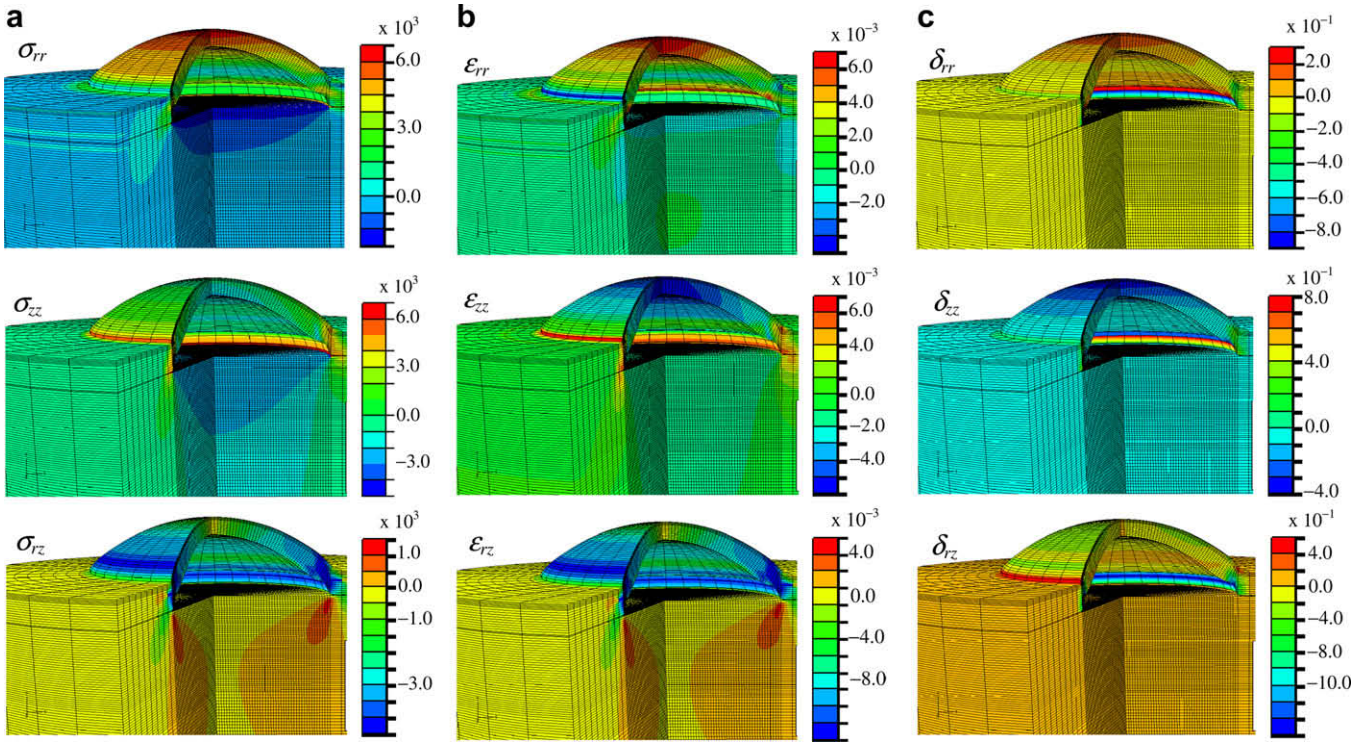

Fig. 10. FEM simulation results of He-blisters, showing distributions of (a) stress (σ_{ij}) in units of Pa; (b) elastic strain (ε_{ij}); and (c) plastic strain (δ_{ij}).

Table 2
Mechanical and structural parameters used for the FEM simulations of blister shape: E = Young's modulus; Y = yield stress; t = blister height; and r = radius of blister base.

SCW specimen # and irradiation parameters	E (GPa)	Y (GPa)	t (nm)	r (nm)
Specimen #2(~350 K) 1.5 keV/H^+ and 1.0×10^{23} H^+/m^2	520	5.0	100	300
Specimen #8 (~300 K)5 keV He^+ and 5.0×10^{21} He^+/m^2	690	6.6	100	500

Table 3
Summary of parameters used for estimating the number of H and He atoms contained in blisters. (i) Parameters derived from FEM simulations: P = internal pressure; V = internal volume. (ii) The number density of blisters, ρ, was measured from GIEM images. (iii) The number of atoms contained in a blister, n, and areal number density of gas atoms involved in blister formation, N_{calc}, were calculated from these values. (iv) Also shown is the areal number density of retained D [41] and He [28,42,43] measured in D/He retention experiments.

SCW Specimen # and irradiation parameters	P (GPa)	V (nm^3)	ρ (m^{-2})	n	N_{calc} (m^{-2}) FEM	N_{exp} (m^{-2}) (from literature)
Specimen #2 (~350 K) 1.5 keV/H^+ and 1.0×10^{23} H^+/m^2	1.7	1.4×10^7	3×10^{12}	5.0×10^8	3.0×10^{21}	$\sim 5 \times 10^{20}$ D^+/m^2 (1 keV D^+) [41]
Specimen #8 (~300 K) 5 keV He^+ and 5.0×10^{21} He^+/m^2	1.6	1.1×10^8	1×10^{12}	2.6×10^9	2.6×10^{21}	1×10^{21} He^+/m^2 (0.5 and 2 keV projected to 5 keV He^+) [28] 1×10^{21} He^+/m^2 (5 keV He^+) [42] 2×10^{21} He^+/m^2 (8 keV He^+) [43]

FEM calculations, i.e., the pressures needed to reproduce the experimentally observed blister shapes, were 1.7 and 1.6 GPa for the H- and He-blisters, respectively.

From Figs. 9 and 10, we observe that elastic strains dominate in the blister formed by H^+ irradiation, while plastic strains are significant in the blister formed by He^+ irradiation. As expected, the stresses are concentrated along the edges of the internal openings and the simulation failed for larger internal pressures both in H- and He-blisters. This means that the size of blisters in tungsten is controlled by the mechanical strength limit. For D^+ irradiation the dose dependence data of the mechanical parameters are available only up to 25 dpa [40], whereas the fluence of 1.0×10^{23} D^+/m^2 to form D-blisters corresponds to more than 100 dpa. We attempted to reproduce the D-blister shape, using the values at 25 dpa, which turned out to fail for any internal pressure.

From the derived gas pressures, the number of molecules involved in the internal volume of the blister was estimated using the van der Waals equation of state:

$$n^3 - \frac{V}{b}n^2 + \frac{(RT + PV)}{ab}n - \frac{PV^3}{ab} = 0, \quad (1)$$

where n, V, P, T, and R are the number of molecules, volume, pressure, absolute temperature, and gas constant, respectively. The van der Waals constants for H_2 are: $a = 0.245$ atm dm^6 mol^{-2} and $b = 0.0267$ dm^3 mol^{-1}; similarly, for He: $a = 0.034$ atm dm^6 mol^{-2} and $b = 0.0238$ dm^3 mol^{-1}. The approximate total number of incident beam atoms per unit area, N_{calc}, contained in all blisters over this unit area was estimated from the calculated number of gas atoms, n, in a typical blister volume, and the observed number density of blisters per unit area, ρ. These calculated amounts of H and He atoms (N_{calc}) in the blisters, together with experimental measurements (N_{exp}) under similar irradiation conditions for D^+ [41] and He^+ [28,42,43] retention in tungsten, are given in Table 3.

In the case of hydrogen, the calculated amount is about six times larger than the experimentally measured D retention for 1 keV D^+ irradiation of PCW [41]. (We note that D retention is used for this comparison because no H retention data are available.) For He the calculated amount is about a factor of 2.6 larger than the experimental measurements [28,42,43]. The observed differences might be attributed to the escape of He atoms and H_2 molecules (in the case of hydrogen) from the blisters during and shortly after irradiation, so these atoms/molecules would not have been detected during the subsequent TDS measurements. Escape of atoms/molecules might have been caused by structural changes during irradiation, such as transition from single crystal to polycrystalline or amorphous, and the possible formation of nano-size cracks. While these atom/molecule losses from the blisters would lead to lower amounts of He/hydrogen measured by TDS, they would not affect the calculated He/hydrogen accumulation in the blisters, which is based on measured blister shapes, sizes and density. In both cases (H and He), the measured retained amounts are 2.6–6 times lower than the calculated amounts. Considering uncertainties in both the experimental measurements and modelling assumptions, we do not consider the difference between H and He to be significant.

6. Summary and conclusions

We have used non-destructive grazing-incidence electron microscopy (GIEM) to examine the structure and morphology of surface blisters formed in tungsten during H^+, D^+ and He^+ irradiations. GIEM images of 1.5 keV D^+-irradiated PCW clearly show that blister formation occurs at about 50-150 nm depth, which is greater than the implanted D^+ ion distribution (<40 nm). Electron diffraction patters show that the PCW specimen changed to an 'amorphous' structure.

Blister formation was also observed with GIEM for single crystal tungsten irradiated with H^+, D^+, and He^+. The critical ion fluence for blister formation in SCW is estimated to be $\sim 10^{23}$ $H^+(D^+)/m^2$ for H(D) and $\sim 10^{21}$ He^+/m^2 for He. The size of the blisters and their skin structure depends on the irradiating conditions. However, in contrast to the case of PCW, the internal structure of the blisters in SCW was more difficult to discern even with the use of 1 MeV electrons, implying larger blister skin thicknesses. For SCW an amorphous blister structure is observed for D^+ irradiation at ~400 K to a fluence of 10^{23} D^+/m^2. However, as the fluence is increased to 10^{24} D^+/m^2 the presence of fine polycrystalline particles is evident, implying that some re-crystallization might have occurred. At the same ion energy, blister size is larger for D^+ than for H^+ irradiation of SCW. At the same ion energy and irradiation temperature the blister size in SCW increases with increasing D^+ fluence, while for the same D^+ energy and fluence, the growth of blisters – both height and density – appears to be suppressed with increasing irradiation temperature.

The blister morphology and gas retention in tungsten depend on the irradiation-induced changes in the mechanical properties of the surface layer. Based on the observed blister features, FEM simulations were performed to reproduce the blister shapes, by which the internal pressures and gas retention in the blisters were estimated. From the GIEM images and FEM calculations we have estimated the number of H and He atoms accumulated in the blisters. When compared to published experimental retention results, the calculated values are found to be higher than those measured by TDS in D and He retention experiments. The observed differences might be attributed to the escape of atoms from the blisters during and shortly after irradiation, so these atoms would not be detected during the subsequent TDS measurements.

Here, we propose a model for the blistering process based on the hypothesis that hydrogen introduced in the surface layer by prolonged irradiation pushes the preexisting distribution of trapped atoms deeper into the specimen. Verification of this model would require the use of cross-sectional TEM to observe any accumulated hydrogen at the interface between the highly defective (or amorphous) surface layer and the original single crystal substrate. However, we have not yet succeeded in preparing a

specimen suitable for XTEM due to tungsten's hardness and high atomic weight.

Acknowledgments

We are very grateful to Dr S. Arai of EcoTopia Science Institute, Nagoya University for his support in HVEM operation. This work is partly supported by Grant-in-Aid for Scientific Research of MEXT (Kibankenkyu A, No.17206063), Japan, and the Natural Sciences and Engineering Research Council of Canada. We also thank Dr Michael Poon (University of Toronto) for his help in the implantation of the PCW specimen.

References

[1] D.J. Mazey, J. Nucl. Mater. 174 (1990) 196.
[2] H. Verbeek, W. Eckstein, Application of Ion Beam to Metals, Plenum, New York, 1974. p. 609.
[3] S. Muto, T. Matsui, T. Tanabe, Jpn. J. Appl. Phys. 39 (2000) 3555.
[4] S. Muto, T. Matsui, T. Tanabe, J. Nucl. Mater. 290–293 (2001) 131.
[5] S. Igarashi, S. Muto, T. Tanabe, T. Maruyama, Mater. Trans. JIM 42 (2001) 2131.
[6] S. Igarashi, S. Muto, T. Tanabe, J. Aihara, K. Hojou, Surf. Coat. Technol. 158–159C (2002) 421.
[7] S. Igarashi, S. Muto, T. Tanabe, T. Maruyama, J. Nucl. Mater. 307–311 (2002) 1126.
[8] S. Muto, N. Enomoto, Mater. Trans. 46 (2005) 2117.
[9] S. Nakano, S. Muto, T. Tanabe, Mater. Trans. 47 (2006) 112.
[10] S. Muto, T. Tanabe, T. Maruyama, Mater. Trans. 44 (2003) 2599.
[11] G. Federici, C.H. Skinner, J.N. Brooks, et al., Nucl. Fus. 41 (2001) 1967.
[12] H. Bolt, V. Barabash, W. Krauss, J. Linke, R. Neu, S. Suzuki, N. Yoshida, ASDEX Upgrade Team, J. Nucl. Mater. 329–333 (2004) 66.
[13] K. Tokunaga, M. Takayama, T. Muroga, N. Yoshida, J. Nucl. Mater. 220–222 (1995) 800.
[14] S. Nagata, K. Takahiro, S. Horiike, S. Yamaguchi, J. Nucl. Mater. 266–269 (1999) 1151.
[15] V. Kh. Alimov, K. Ertl, J. Roth, J. Nucl. Mater. 290–293 (2001) 389.
[16] A.A. Haasz, M. Poon, J.W. Davis, J. Nucl. Mater. 266–269 (1999) 520.
[17] A.A. Haasz, J.W. Davis, M. Poon, R.G. Macualy-Newcombe, J. Nucl. Mater. 258–263 (1998) 889.
[18] R. Sakamoto, T. Muroga, N. Yoshida, J. Nucl. Mater. 220–222 (1995) 819.
[19] V. Kh. Alimov, J. Roth, M. Mayer, J. Nucl. Mater. 337–339 (2005) 619.
[20] Y. Ueda, T. Funabiki, T. Shimada, K. Fukumoto, H. Kurishita, M. Nishikawa, J. Nucl. Mater. 337–339 (2005) 1010.
[21] W. Wang, J. Roth, S. Lindig, C.H. Wu, J. Nucl. Mater. 299 (2001) 124.
[22] K. Tokunaga, M.J. Baldwin, R.P. Doerner, et al., J. Nucl. Mater. 337–339 (2005) 887.
[23] H. Iwakiri, K. Yasunaga, K. Morishita, N. Yoshida, J. Nucl. Mater. 283–287 (2000) 134.
[24] S. Nagata, B. Tsuchiya, T. Sugawara, N. Ohtsu, T. Shikama, Nucl. Instrum. and Meth. B 190 (2002) 652.
[25] D. Nishijima, M.Y. Ye, N. Ohno, S. Takamura, J. Nucl. Mater. 313–316 (2003) 97.
[26] K. Tokunaga, S. Tamura, N. Yoshida, K. Ezato, M. Taniguchi, K. Sato, S. Suzuki, M. Akiba, J. Nucl. Mater 329–333 (2004) 757.
[27] A.A. Haasz, J.W. Davis, Nucl. Instrum. and Meth. B 83 (1993) 117.
[28] H.T. Lee, A.A. Haasz, J.W. Davis, R.G. Macaulay-Newcombe, J. Nucl. Mater. 360 (2007) 196.
[29] J.F. Ziegler, M.D. Ziegler, J.P. Biersack, SRIM version 2006, 02.
[30] R. Uyeda, M. Nonoyama, Jpn. J. Appl. Phys. 17 (1968) 200.
[31] G.-N. Luo, W.M. Shu, M. Nishi, J. Nucl. Mater. 347 (2005) 111.
[32] N. Yoshida, H. Iwakiri, K. Tokunaga, T. Baba, J. Nucl. Mater. 337–339 (2004) 946.
[33] B.M.U. Scherzer, Sputtering by Particle Bombardment II: Topics in Applied Physics, vol. 52, Springer-Verlag, Berlin, 1983, p. 334.
[34] M. Poon, A.A. Haasz, J.W. Davis, J. Nucl. Mater. 374 (2008) 390.
[35] H. Eleveld, A. vanVeen, J. Nucl. Mater. 191–194 (1992) 433.
[36] V. Kh. Alimov, J. Roth, Phys. Scr. T128 (2007) 6.
[37] M. Poon, R.G. Macaulay-Newcombe, J.W. Davis, A.A. Haasz, J. Nucl. Mater. 307–311 (2002) 723.
[38] M. Poon, R.G. Macaulay-Newcombe, J.W. Davis, A.A. Haasz, J. Nucl. Mater. 337–339 (2005) 629.
[39] http://www.simulia.com.
[40] S.A. Maloy, M.R. James, W. Sommer Jr., G.J. Willcutt Jr., M. Lopez, T.J. Romero, M.B. Toloczko, J. Nucl. Mater. 343 (2005) 219.
[41] A.A. Haasz, J.W. Davis, J. Nucl. Mater. 241–243 (1997) 1076.
[42] T. Hino, Y. Yamauchi, Y. Hirohata, J. Nucl. Mater. 266–269 (1999) 538.
[43] Zhang Fu, N. Yoshida, H. Iwakiri, Zengyu Xu, J. Nucl. Mater. 329–333 (2004) 692.